Rotational and orientational behaviour of three-dimensional spheroidal particles in Couette flows

By DEWEI QI[1] AND LI-SHI LUO[2]

[1] Department of Paper and Printing Science and Engineering, College of Applied Science and Engineering, Western Michigan University, Kalamazoo, MI 49008, USA

[2] ICASE, Mail Stop 132C, NASA Langley Research Center, Hampton, VA 23681-2199, USA

This paper reports the results of lattice Boltzmann simulations of the rotation behaviour of neutrally buoyant spheroidal particles in a three-dimensional Couette flow. We find several distinctive states depending on the Reynolds number range and particle shape. As the Reynolds number increases, rotation may change from one state to another. For a prolate spheroid, two rotation transitions are found. In the low Reynolds number range $0 < R < R_1 \approx 205$, the prolate spheroid rotates around its minor axis, which is parallel to the vorticity vector of the flow. The rate of rotation is a periodic function of time. In the intermediate Reynolds number range $R_1 < R < R_2 \approx 345$, the prolate spheroid precesses about the vorticity direction with a nutational motion. The angular velocities are periodic functions of time. The mean nutation angle between the major axis and the vorticity increases monotonically as the Reynolds number increases. In the high Reynolds number range $R_2 < R < 467$, the prolate spheroid rotates with a constant rate around its major axis, which is parallel to the vorticity. For an oblate spheroid, only one rotation transition is observed. In the lower Reynolds number range $0 < R < R'_1 \approx 220$, the oblate spheroid finally spins with a constant rate around its minor axis (the symmetric axis of the revolution), which is parallel to the vorticity vector. In the higher Reynolds number range $220 \approx R'_1 < R < 467$, the oblate spheroid still spins with a constant rate around its minor axis but there is a finite inclination angle between the minor axis and the vorticity vector. This angle increases as the Reynolds number increases.

1. Introduction

Suspensions of solid particles in fluids are ubiquitous in many industries, such as printing and paper-making, petroleum, bioengineering, pharmaceuticals and food processing. In the paper-making industry, a suspension consisting of fillers, pigments and binders is coated on the paper surface to improve the smoothness and optical properties of the paper. These filler particles in the suspension are subjected to a shear force in a coater. The shear flow affects the distribution of the particles due to their motion and determines the quality of the paper surface to some extent. Most particles in realistic situations are non-spherical, or even irregular. This complex geometry strongly affects the particle–fluid and particle–particle interactions and thus complicates the structures of both the flows and particle clusters. Therefore, an understanding of the dynamic behaviour of particulate suspensions of non-spherical particles in shear flows is important for various engineering applications.

The motion of non-spherical particles in a shear flow at very low Reynolds numbers has been studied for a long time (cf. e.g. the review by Leal 1980). Jeffery (1922) investigated the rotational behaviour of a single ellipsoid in a simple shear flow at zero Reynolds number. The inertial effect was completely neglected in Jeffery's study, which used the quasi-steady approach by assuming that the pressure is the only driving force for rotation. Jeffery obtained a set of differential equations for the rotation of an ellipsoid with analytic solutions depending on the initial conditions. Jeffery therefore concluded that the rotation of an ellipsoid is indeterminant. In order to definitively determine the final orbit of an ellipsoid, Jeffery hypothesized that "The particle will tend to adopt that motion which, of all the motions possible under the approximated equations, corresponds to the least dissipation of energy."

Jeffery's (1922) analytic work has had a strong influence and has spawned numerous experimental and theoretical research efforts. Taylor (1923) reported that a prolate or oblate spheroid in a Couette flow of an extremely viscous fluid adopted the orbit of minimum energy dissipation, and thus confirmed Jeffery's hypothesis experimentally. However, in experimental work on a single rods or discs in both Couette and Poiseuille flows, Karnis, Goldsmith & Mason (1963, 1966) conclusively showed that the inertial effect at Reynolds number $R \sim O(10^{-3})$ is sufficient to force non-spherical particles in a shear flow to a final orientation that is different from Jeffery's hypothesis. Theoretical studies were also made to understand the effect of inertia of non-spherical particles on their motion in fluids. Although the experimental results of Karnis *et al.* (1963, 1966) were qualitatively confirmed by the analysis of Harper & Chang (1968) and Leal (1975), their analysis was a generalization of Saffman's (1965) work on the effect of inertia on a sphere in Poiseuille flow, and was based on a perturbation theory limited to Reynolds numbers $R < 1$. Therefore their analysis cannot be applied to large Reynolds number cases.

Recently, there has been an increase in the study of particulate suspensions with use of direct numerical simulations. Feng & Joseph (1995) simulated the dynamic behaviour of a single ellipse in a planar Couette flow at the Reynolds number $R = 1$ by using a finite element method. Their numerical results were essentially consistent with Jeffery's theory. More recently, with a lattice Boltzmann method, Ding & Aidun (2000) simulated a single circular cylinder (with $0 < R \leqslant 320$) and elliptical cylinder (with $5 \leqslant R \leqslant 50$) in planar Couette flow, as well as a single oblate spheroid ($5 \leqslant R \leqslant 90$) with its diameter fixed in the direction of the flow vorticity vector in three-dimensional Couette flow. Their numerical findings for a circle suspended in planar Couette flow have been observed experimentally by Zettner & Yoda (2000, 2001). Despite all the progress that has been made in the area, for finite particle Reynolds number, when the nonlinear inertial effect becomes important, the dynamics of non-spherical particulate suspensions, even the simplest case of a single particle in shear flows, is not well understood. Essentially, there are neither experimental nor theoretical results available for a non-spherical particulate suspension in a three-dimensional Couette flow at sufficiently large Reynolds numbers.

The present work investigates the rotational behaviour of a non-spherical particle in a three-dimensional Couette flow at particle Reynolds numbers up to 467 by using a lattice Boltzmann equation (LBE) with fifteen discrete velocities (the D3Q15 model). Within this range of Reynolds numbers ($0 < R \leqslant 467$), we find that the rotation of a spheroid exhibits several distinctive states depending on the Reynolds number range and particle shape. As the Reynolds number changes, the rotation transitions from one state to another.

The remainder of this paper is organized as follows. Section 2 gives a concise description of the lattice Boltzmann method for fluid flows. Sections 3 and 4 present the numerical results for a single prolate and oblate spheroid in three-dimensional Couette flow, respectively. The rotational behaviour of these non-spherical particles is investigated. In §5 the relative viscosities of a single particle with or without rotational constraints are computed to test the validity of Jeffery's 'minimum energy dissipation' hypothesis at a finite Reynolds number. Section 6 contains discussion and conclusions.

2. Simulation method

The lattice Boltzmann equation (McNamara & Zanetti 1988; Qian, d'Humières & Lallemand 1992; Chen, Chen & Matthaeus 1992; He & Luo 1997*a,b*; Luo 1998, 2000) has been successfully applied to simulate particulate suspensions in flows at finite Reynolds numbers (Ladd 1994*a,b*; Koch & Ladd 1997; Aidun, Lu & Ding 1998; Aidun & Qi 1998; Qi 1997*a,b*, 1999, 2000; Qi & Luo 2002). The lattice Boltzmann equation is a special finite difference form of the Boltzmann equation (He & Luo 1997*a,b*; Junk & Klar 2000; Junk 2001). The particle velocity space is discretized and reduced to a small set of discrete velocities. The spatial discretization is coupled to the temporal discretization and the discrete velocity set such that the physical space becomes a highly symmetric discrete lattice space. The lattice Boltzmann equation with the single relaxation time approximation (Bhatnagar, Gross & Krook 1954) is used here. The moving boundary conditions and calculations of hydrodynamic forces on a solid particle were reported in the articles by Ladd (1994*a,b*), Aidun *et al.* (1998) and Qi (1999, 2000), and will not be repeated here. The same methods are used in this study.

We consider the ellipsoid particle described by

$$\frac{x'^2}{a^2} + \frac{y'^2}{b^2} + \frac{z'^2}{c^2} = 1, \tag{2.1}$$

where a, b and c denote the lengths of three semi-principal axes, and (x', y', z') denotes the body-fixed coordinate system, as opposed to the space-fixed coordinate system (x, y, z). The polar angle between the vorticity vector (z-axis) and the z'-axis of the ellipsoid is θ and the angle between the (x, z)-plane and the (x', z)-plane is ϕ if the body-fixed coordinate system (x', y', z') initially overlaps the space-fixed coordinate system (x, y, z). The rotational angle about the z'-axis is ψ. The stream direction of the Couette flow is along the y-direction, with the shear gradient imposed in the x-direction and the flow vorticity along the z-direction. The mesh of the simulation box is denoted by (N_x, N_y, N_z). Two walls located at $x = 0$ and $x = N_x + 1$ move in opposite directions with speed U as shown in figure 1. Periodic boundary conditions are applied in both the y- and z-directions. The particle Reynolds number is defined by

$$R = \frac{4Gc^2}{\nu}, \tag{2.2}$$

where shear rate $G = 2U/N_x$, c is the length of the semi-major axis and ν is kinematic viscosity. $U \leqslant 0.1$ is used for all the cases to ensure the validity of Galilean invariance in the simulations.

3. Rotation of a prolate spheroid

To study the dynamic rotational behaviour of a neutrally buoyant prolate spheroidal particle in a sufficiently large Reynolds number range, we conducted a number of
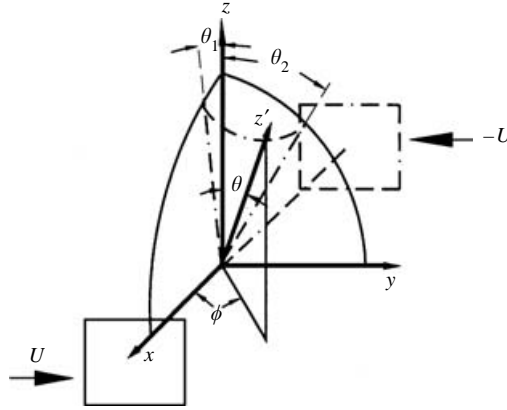
FIGURE 1. The configuration of the Couette flow. The two walls (arbitrarily scaled) at $x = 0$ and $x = N_x + 1$ move at velocity U in opposite directions. The vorticity vector of the flow is in the z-direction. The z'-axis is the revolution axis of the spheroid.

R	(N_x, N_y, Nz)	(a, b, c)	ν
32	64, 64, 64	8, 8, 16	0.1
128	64, 64, 64	8, 8, 16	0.025
170	96, 96, 96	12, 12, 24	0.0282353
200	96, 96, 96	12, 12, 24	0.024
220	96, 96, 96	12, 12, 24	0.021818
240	96, 96, 96	12, 12, 24	0.02
280	112, 112, 112	14, 14, 28	0.02
320	112, 112, 112	14, 14, 28	0.0175
350	112, 112, 112	14, 14, 28	0.016
400	128, 128, 128	16, 16, 32	0.016
410	128, 128, 128	16, 16, 32	0.0156097

TABLE 1. Simulation box and particle sizes and kinematic viscosities for different cases.

simulations at $R = 32, 128, 170, 200, 220, 240, 280, 320, 350, 400$ and 410. The simulation box size, particle sizes and kinematic viscosities are listed in table 1.

The rotational motion of the particle is affected by both the confinement ratio $r_1 = N_x/c$ and the aspect ratio of the particle $r_2 = c/a$. We fixed the ratios at $r_1 = 4$ and $r_2 = 2$ for most cases in this study. The effect of the confinement ratio on the rotation behaviour will be discussed at the end of this section.

We observe that the final stage in the rotation of a prolate spheroid exhibits three distinctive states within the Reynolds number range $0 < R < 467$. First, in the low Reynolds number range $0 < R < 205$, the prolate spheroid reaches a steady state in which it rotates about its minor axis, which is parallel to the flow vorticity vector; thus the major axis is perpendicular to the vorticity vector, i.e. $\theta = 90°$. The angular velocity vector is $\boldsymbol{\omega} = (\omega_x, \omega_y, \omega_z) = (0, 0, \omega)$, where $\omega = |\boldsymbol{\omega}|$, and the rotational rate $\dot{\phi} = \omega_z$ is periodic in time. We call this rotation state 'tumbling'. In this state, the periodicity of $\dot{\phi}$ monotonically increases as the Reynolds number increases. The angular velocity $\omega = \omega_z = \dot{\phi}$ is shown as a function of time at different Reynolds numbers in figure 2. All systems in this low Reynolds number range have a similar rotational behaviour.
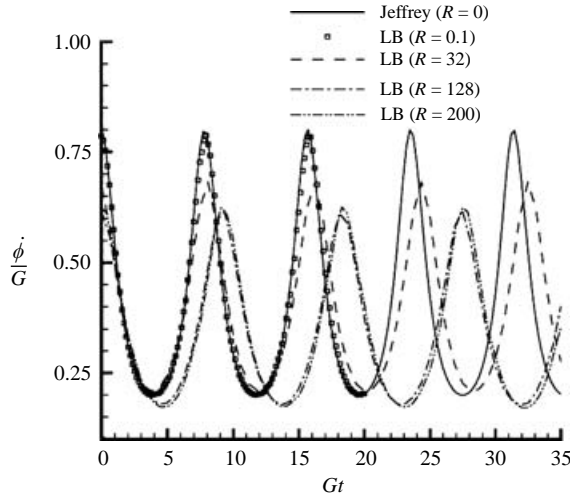
FIGURE 2. The normalized angular velocity $\dot{\phi}/G$ of a prolate spheroid as a function of the dimensionless time Gt in the low Reynolds number range $0 < R < 205$. The LBE simulation results at $R = 0.1, 32, 128, 200$ and the analytic result of Jeffery's theory at $R = 0$ are shown.
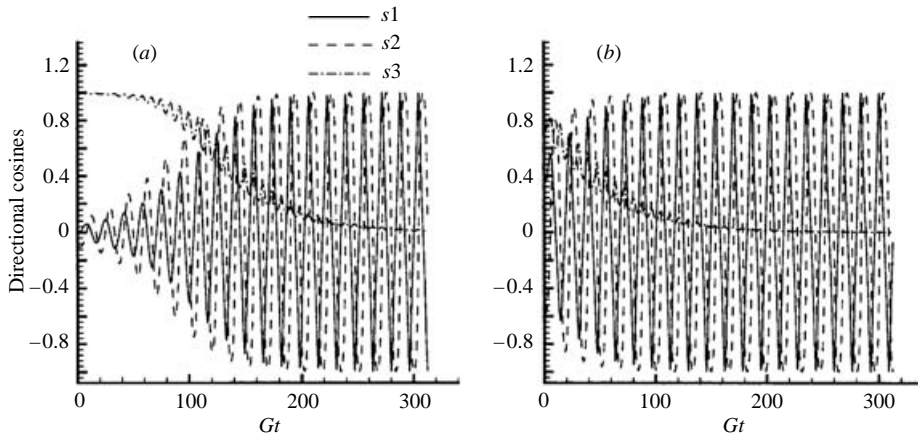

FIGURE 3. Transient behaviour of the directional cosines $(s1, s2, s3) = (\cos\beta, \cos\gamma, \cos\theta)$ of the z'-axis for the prolate spheroid at $R = 32$ with two different initial orientations: (a) $(\theta_0, \phi_0, \psi_0) = (5.73°, -87.1°, 0°)$ and (b) $(43°, -58.5°, 121.5°)$.

To demonstrate the dynamic behaviour of the spheroid in the low Reynolds number range, in figure 3 we show the evolution of the directional cosines $(s1, s2, s3) = (\cos\beta, \cos\gamma, \cos\theta)$ at $R = 32$ for two different initial conditions $(\theta_0, \phi_0, \psi_0) = (5.73°, -87.1°, 0°)$ and $(43°, -58.5°, 121.5°)$. For the first initial condition, the major axis of the spheroid (the z'-axis) is almost parallel to the flow vorticity vector. This configuration is unstable. The spheroid major axis eventually turns perpendicular to the vorticity vector and rotates on the shear plane perpendicular to the vorticity vector, as clearly shown in figure 3. In the final state, angle θ approaches $90°$ ($\cos\theta \to 0$) regardless of the initial orientation of the particle. It is clear that the final orientation of the particle is independent of the initial conditions.
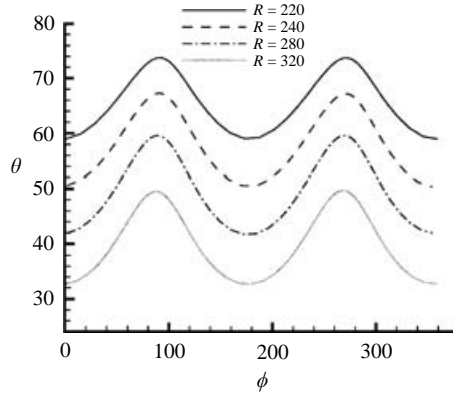
FIGURE 4. The polar angle θ of the z'-axis vs. angle ϕ over one period of the rotation for the prolate spheroid at Reynolds numbers $R = 220$, 240, 280 and 320.
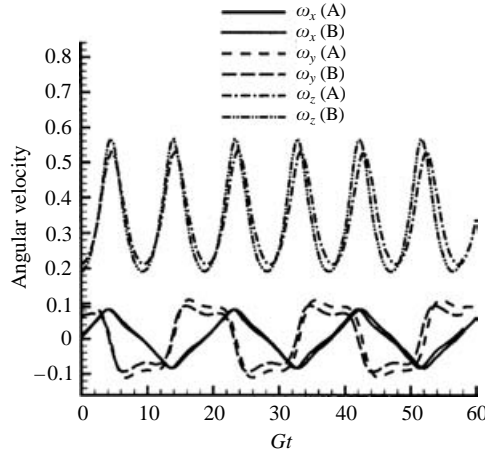

FIGURE 5. The periodic behaviour of the rotational motion of the prolate spheroid at $R = 240$ (in the intermediate Reynolds number range). The angular velocity $\boldsymbol{\omega} = (\omega_x, \omega_y, \omega_z)$ as a function of the dimensionless time Gt. The box mesh is $(96, 96, 96)$ for simulation A and $(96, 112, 112)$ for simulation B while the particle size is $(a = 12, b = 12, c = 24)$.

As the Reynolds number increases beyond the first transition Reynolds number $R_1 \approx 205$, the rotation evolves to a different state. In this intermediate Reynolds number range $205 < R < 345$, the major axis of the prolate spheroid (z'-axis) precesses around the flow vorticity vector with a nutation, i.e. the inclination angle θ between the major axis and the vorticity varies periodically in time, and is confined between a minimum $\theta_1 > 0°$ at $\phi = 0°$ and $180°$ and a maximum $\theta_2 < 90°$ at $\phi = 90°$ and $270°$. The end of the major or revolution axis of the prolate spheroid appears to describe a spherical ellipse with its major axis at $\phi = 90°$ and minor axis at $\phi = 0°$. Figure 4 shows the angle θ vs. angle ϕ for one period of the rotation for $R = 220$, 240, 280 and 320. In this state, all three components of the angular velocity $\boldsymbol{\omega}$ of the spheroid are not zero and are periodic in time, as shown in figure 5 for the case $R = 240$. We simply call this state 'precessing and nutating'. The mean value of θ decreases monotonically as the Reynolds number increases. That is, the major axis
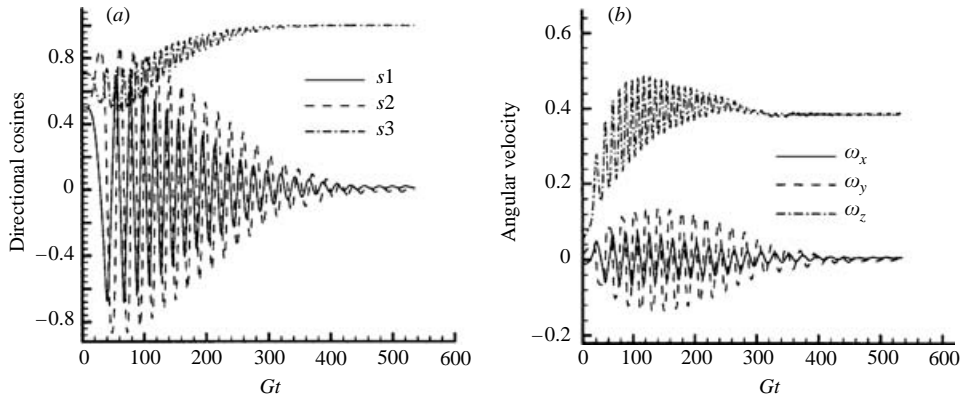
FIGURE 6. Transient rotational behaviour of the prolate spheroid at $R = 350$. (*a*) The direction cosines $(s1, s2, s3) = (\cos\beta, \cos\gamma, \cos\theta)$ of the z'-axis. (*b*) The angular velocity $\boldsymbol{\omega} = (\omega_x, \omega_y, \omega_z)$.

of the spheroid more closely aligns itself with the vorticity vector as the Reynolds number increases.

When the Reynolds number further increases beyond a second transition Reynolds number ($R_2 \approx 345$), the prolate spheroid finally rotates at a constant rate around its major axis which is parallel to the vorticity vector of the flow, i.e. $\theta = 0°$. We call this rotation state 'rolling'. Figure 6(*a*) shows the dynamic orientational behaviour of the prolate spheroid at $R = 350$, a typical case in the high Reynolds number range $R > 345$, and figure 6(*b*) shows the transient behaviour of the angular velocity at the same Reynolds number.

In summary, we have observed two transitions in the final rotational state for the prolate spheroid as the Reynolds number continuously varies from 0 to 467. First, in the low Reynolds number range, the prolate spheroid rotates around its minor axis which is parallel to the flow vorticity. The first transition occurs at $R_1 \approx 205$. In the intermediate Reynolds number range $205 < R < 345$, the prolate spheroid precesses around the flow vorticity vector with a nutation. The inclination angle θ between the major axis and vorticity vector is between $\theta_1 > 0°$ and $\theta_2 < 90°$, and the mean value of θ decreases monotonically as the Reynolds number increases. The second transition takes place at $R_2 \approx 345$. In the high Reynolds number range $345 < R < 467$, the prolate spheroid finally rotates at a constant rate around its major axis, which is parallel to the flow vorticity. In short, as the Reynolds number increases, the rotation of a prolate spheroid transits from a tumbling state to a precessing and nutating state, then to a rolling state.

It is well known that the confinement ratio r_1 will affect the rotation rate of a particle (Poe & Acrivos 1975). The effects of this ratio on the rotation states are briefly and qualitatively studied here. Three simulations of a single prolate ellipsoid are conducted at the same Reynolds number $R = 240$ with different confinement ratios of $r_1 = 3, 4$ and 4.5. The results for θ against ϕ in one period of rotation are plotted and compared in figure 7. As shown before, the prolate ellipsoid is in a precessing and nutating state at $R = 240$ when $r_1 = 4$. As the confinement ratio is reduced to $r_1 = 3$, the particle rotates in a tumbling state ($\theta \approx 90°$). This means that for the particle to be in a precessing and nutating state requires a higher Reynolds number for $r_1 = 3$ than for $r_1 = 4$. As r_1 increases to 4.5, the particle moves into
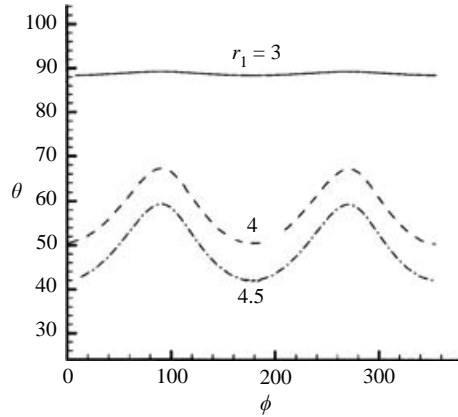
FIGURE 7. The polar angle θ of the z'-axis vs. angle ϕ over one period of the rotation for the prolate spheroid at Reynolds number $R = 240$ with confinement ratios $r_1 = 3, 4$ and 4.5.

a precessing and nutating state. However, the mean value of θ is less for $r_1 = 4.5$ than for $r_1 = 4$. In other words, the long axis of the particle is closer to the vorticity direction ($\theta = 0°$) for $r_1 = 4.5$ than for $r_1 = 4$. These results suggest that as the confinement ratio is reduced, the transition Reynolds number shifts to a higher value. Inversely, as the confinement ratio increases the transition Reynolds number shifts to a lower value. There is no attempt made here to locate the transition Reynolds number for each confinement ratio due to limits on computational time.

4. Rotation of an oblate spheroid

We have also simulated the case of a single neutrally buoyant oblate spheroid. In these simulations, the z'-axis is the minor or revolution axis. We find that in a low Reynolds number range ($0 < R < 220$) the oblate spheroid eventually spins at a constant rate around its minor axis, which is parallel to the flow vorticity vector ($\theta = 0°$). We call this state 'spinning'. The results for a typical case of $R = 32$ in the low Reynolds number range are shown in figure 8(a) for orientation evolution and in figure 8(b) for angular velocities. In this case, the simulation box size and particle sizes are (64, 64, 64) and ($a = 16, b = 16, c = 8$) respectively.

A transition occurs when the Reynolds number increases beyond the first transition Reynolds number $R_1 \approx 220$. When $R > 220$, the oblate spheroid still spins about its minor axis (z'-axis), but the minor axis has a finite inclination angle θ with the vorticity. We call this 'inclined spinning'. Figure 9(a) shows that after a transient period of time, the orientation of the oblate spheroid reaches a steady state and the inclined angle θ at $R = 400$ is approximately 16.52°. Figure 9(b) shows that the angular velocity $\boldsymbol{\omega} = (\omega_x, \omega_y, \omega_z)$ becomes a constant vector. The inclination angle θ increases monotonically as R increases. Although we anticipate that, at a sufficiently large Reynolds number beyond a second transition Reynolds number R_2; the oblate spheroid would eventually rotate (tumbling) about its diameter which is parallel to the flow vorticity vector, i.e. $\theta = 90°$, such very high Reynolds numbers have not been reached.

To check numerical accuracy, the effect of the size of the particle and simulation box on results has been investigated for small particles. For instance, the simulation box size (64, 64, 64) and particle size ($a = 10.9, b = 10.9, c = 5.45$) of an oblate spheroid
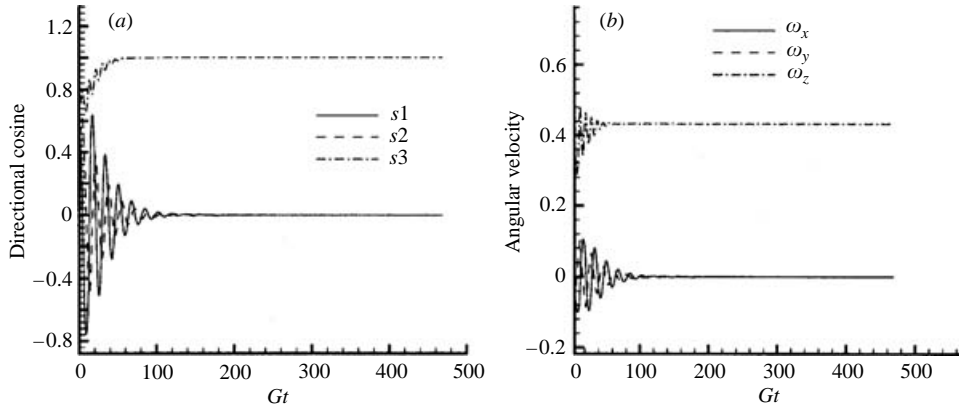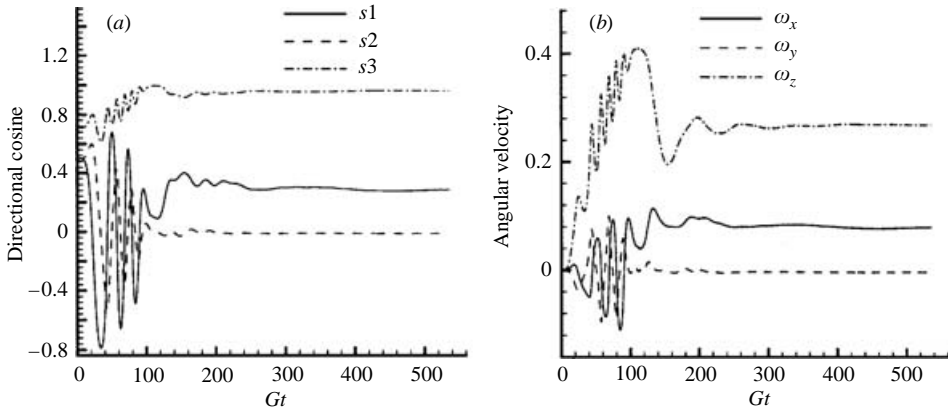
FIGURE 8. Transient rotational behaviour of the oblate spheroid at $R = 32$. (*a*) The direction cosines $(s1, s2, s3) = (\cos\beta, \cos\gamma, \cos\theta)$ of the z'-axis. (*b*) The angular velocity $\boldsymbol{\omega} = (\omega_x, \omega_y, \omega_z)$.

FIGURE 9. Transient rotational behaviour of the oblate spheroid at $R = 400$. (*a*) The direction cosines $(s1, s2, s3) = (\cos\beta, \cos\gamma, \cos\theta)$ of the z'-axis. (*b*) The angular velocity $\boldsymbol{\omega} = (\omega_x, \omega_y, \omega_z)$.

were increased to $(96, 96, 96)$ and $(a = 16.35, b = 16.35, c = 8.175)$, respectively, while the Reynolds number is the same at $R = 14.85$. Thus, $U = 0.1$ for the former simulation and $U = 0.066661$ for the latter one while $\nu = 0.1$ for both. The results for the directional cosines are shown in figure 10. The results for these two different box sizes do not display any significant difference, indicating a good convergence in the simulations. More importantly, although there are two different wall velocities the results are almost the same. It appears that the effect of velocity $U = 0.1$ at the walls on Galilean invariance is very small. Further, the effect of different size boxes on rotation of a solid particle is also examined. For the case of $R = 240$, the angular velocities of a particle of size $(a = 12, b = 12, c = 24)$ in the simulation boxes A of $(96, 96, 96)$ and B of $(96, 112, 112)$ were compared in figure 5 above; $\nu = 0.2$ for both the simulations. It is shown that the size has an effect on the results since the corresponding curves in the two simulations are shifted. However, the precessing and
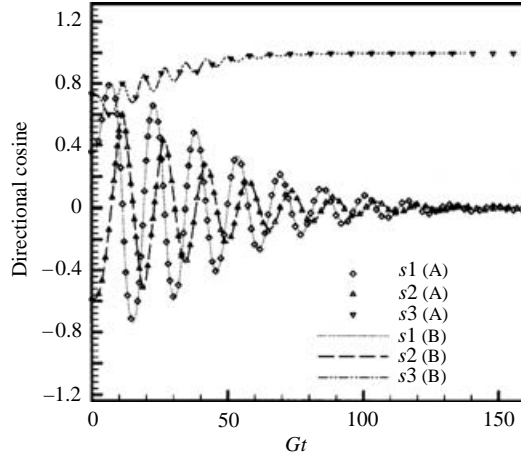
FIGURE 10. The directional cosines of the z'-axis of the oblate spheroid as a function of time at $R = 14.85$ for two different sizes of simulation box and particle: $(64, 64, 64)$ and $(a = 10.9, b = 10.9, c = 5.45)$ for simulation A and $(96, 96, 96)$ and $(a = 16.35, b = 16.35, c = 8.175)$ for simulation B.

nutating behaviour at this Reynolds number is not altered. Thus, the size effect may cause the transition Reynolds number to move to a higher value. Therefore, final transition Reynolds numbers should be determined by experiments, not by numerical simulations alone.

5. Energy dissipation

According to Jeffery's hypothesis, the final rotational state of a non-spherical particle is determined by the principle of minimum energy dissipation. To test Jeffery's hypothesis, we conducted the following simulations with a single prolate spheroid of size $(a = 6, b = 6, c = 12)$ with the simulation box $(64, 64, 64)$. We either fix the major axis of the prolate spheroid to be parallel to the flow vorticity vector $(\theta = 0°)$ so that the number of rotational degrees of freedom of the spheroid is reduced to one or allow the spheroid to rotate in the three-dimensional rotational space without any constraints. We measure the relative viscosity of the system of the suspension:

$$\mu_r = \frac{\langle \sigma \rangle}{\rho \nu G}, \tag{5.1}$$

where $\langle \sigma \rangle$ is the average shear stress. The prolate spheroid with no constraints evolves to a final tumbling state around its minor axis, which is along the vorticity direction in the low Reynolds range $(R < 205)$, i.e. the prolate spheroid rotates about its minor axis which is parallel to the flow vorticity vector $(\theta = 90°)$. At the Reynolds number $R = 0.1$, the relative viscosity is $\mu_r = 1.026$ for the spheroid with the constraint of $\theta = 0°$ and $\mu_r = 1.033$ for the unconstrained spheroid (with a final orientation of $\theta = 90°$). We conducted the same simulation at $R = 18$, and obtained $\mu_r = 1.054$ for the constrained system and $\mu_r = 1.069$ for the unconstrained system. Obviously, the final rotation state with $\theta = 90°$ has a higher energy dissipation than that with $\theta = 0°$. Therefore, our results at finite Reynolds numbers conclusively invalidate Jeffery's hypothesis.

6. Discussions and conclusions

In the light of the present results, we would like to comment on the recent numerical work of Aidun *et al.* (1998) and Ding & Aidun (2000) and the experimental work of Zettner & Yoda (2001). Aidun *et al.* (1998) and Ding & Aidun (2000) reported that when the Reynolds number increased to a critical value, the ellipsoid rotation was stopped at a critical Reynolds number R_c due to the effects of streamline separation that generated a negative torque on the non-spherical particles. The critical Reynolds number in Ding & Aidun (2000) was $R_c = 81$ for a three-dimensional oblate ellipsoid and $R_c = 29$ for a two-dimensional elliptical particle. Their numerical results are in good agreement with Zettner & Yoda's experimental results. We repeated the simulations of Ding & Aidun (2000) and confirmed their findings. However, when a three-dimensional spheroid is allowed to freely rotate in six-dimensional space, our results show that the negative torque effect on rotation due to streamline separation is never strong enough to stop the rotation.

It is important to point out some differences between the present work and that mentioned above. First, in the simulations of Ding & Aidun the oblate ellipsoidal particle was forcibly rotated around its major axis, which was fixed in the vorticity vector direction. This is not the final orientation. Second, although three-dimensional geometry was used in their simulation, it was essentially in a two-dimensional rotary space because the major axis was always fixed in the vorticity vector direction or the z-axis direction. Zettner & Yoda (2001) had a similar experimental setting. In the present study, the particle is allowed to freely move and rotate in a three-dimensional setting without any artificial constraint. The final rotation state is fully determined by the six-dimensional equations of the motion of the particle subjected to the influence of hydrodynamic forces and the particle finally reaches a natural orientation.

To the best of our knowledge, there were neither experimental nor theoretical results available for three-dimensional non-spherical suspensions at sufficiently large Reynolds numbers in Couette flows. Therefore, we have investigated the rotational behaviour of a single prolate or oblate spheroid in a three-dimensional Couette flow for particle Reynolds numbers up to 467. We found that the rotation of a prolate spheroid has three distinctive states depending on the Reynolds number. In the low Reynolds number range $0 < R < R_1 \approx 205$, the prolate spheroid rotates around its minor axis, which is parallel to the vorticity vector of the Couette flow; thus the major axis of the spheroid remains perpendicular to the flow vorticity vector. At $R = R_1 \approx 205$ a rotation transition occurs. In the intermediate Reynolds number range $R_1 < R < R_2$ ($R_2 \approx 345$), the spheroid precesses about the flow vorticity vector with a nutation ($0° < \theta_1 < \theta < \theta_2 < 90°$). At $R = R_2 \approx 345$, a second transition takes place. In the high Reynolds number range $R > R_2$, the spheroid rolls about its major axis which is parallel to the flow vorticity vector.

For an oblate spheroid, we observed that in the low Reynolds number range $0 < R < R_1 \approx 220$, it spins about its minor axis at a constant angular velocity, and the minor axis is parallel to the flow vorticity vector so that the diameter of the oblate spheroid is perpendicular to the flow vorticity vector. When the Reynolds number increases beyond a critical value of $R_1 \approx 220$, the oblate spheroid in its final state still spins about its minor axis at a constant angular velocity, but the minor axis has a non-zero inclination angle with the flow vorticity vector.

Finally, we stress that the results of simulations of the final rotational states of a non-spherical particle in a three-dimensional Couette flow, especially the transitions between different rotation states, in the present study are the first and have not been

experimentally observed yet. Our results in the low Reynolds number range confirm the experimental observations by Karnis *et al.* (1963, 1966) for $R = O(10^{-3})$.

REFERENCES

AIDUN, C. K., LU, Y. & DING, E. 1998 Direct analysis of particulate suspensions with inertia using the discrete Boltzmann equation. *J. Fluid Mech.* **373**, 287–311.

AIDUN, C. K. & QI, D. W. 1998 A new method for analysis of the fluid interaction with a deformable membrane. *J. Statist. Phys.* **90**, 145–158.

BHATNAGAR, P. L., GROSS, E. P. & KROOK, M. 1954 A model for collision processes in gases. I. Small amplitude processes in charged and neutral one-component systems. *Phys. Rev.* **94**, 511–525.

CHEN, H., CHEN, S. & MATTHAEUS, W. H. 1992 Recovery of the Navier–Stokes equation using a lattice-gas Boltzmann method. *Phys. Rev.* A **45**, R5339–R5342.

DING, E. & AIDUN, C. K. 2000 The dynamics and scaling law for particles suspended in shear flow with inertia. *J. Fluid Mech.* **423**, 317–344.

FENG, J. & JOSEPH, D. D. 1995 The unsteady motion of solid bodies in creeping flows. *J. Fluid Mech.* **303**, 83–102.

HARPER, E. Y. & CHANG, I.-D. 1968 Maximum dissipation resulting from lift in a slow viscous shear flow. *J. Fluid Mech.* **33**, 209.

HE, X. & LUO, L.-S. 1997a A priori derivation of the lattice Boltzmann equation. *Phys. Rev.* E **55**, R6333–R6336.

HE, X. & LUO, L.-S. 1997b Theory of lattice Boltzmann method: From the Boltzmann equation to the lattice Boltzmann equation. *Phys. Rev.* E **56**, 6811–6817.

JEFFERY, G. B. 1922 The motion of ellipsoidal particles immersed in a viscous fluid. *Proc. R. Lond.* A **102**, 161–179.

JUNK, M. 2001 A finite difference interpretation of the lattice Boltzmann method. *Numer. Meth. Part. Diffl Equat.* **17**, 383–402.

JUNK, M. & KLAR, A. 2000 Discretizations for the incompressible Navier–Stokes equations based on the lattice Boltzmann method. *SIAM J. Sci. Comput.* **22**, 1–19.

KARNIS, A., GOLDSMITH, H. L. & MASON, S. G. 1963 Axial migration of particles in Poiseuille flow. *Nature* **200**, 159–160.

KARNIS, A., GOLDSMITH, H. L. & MASON, S. G. 1966 The flow of suspensions through tubes. V. Inertial effects. *Can. J. Chem. Engng* **44**, 181–193.

KOCH, D. L. & LADD, A. J. C. 1997 Moderate Reynolds number flows through periodic and random arrays of aligned cylinders. *J. Fluid Mech.* **349**, 31–66.

LADD, A. J. C. 1994a Numerical simulations of particulate suspensions via a discretized Boltzmann equation. Part 1. Theoretical foundation *J. Fluid Mech.* **271**, 285–309.

LADD, A. J. C. 1994b Numerical simulations of particulate suspensions via a discretized Boltzmann equation. Part 2. Numerical results. *J. Fluid Mech.* **271**, 311–339.

LEAL, L. G. 1975 The low motion of slender fluid rod-like particles in a second order fluid. *J. Fluid Mech.* **69**, 305.

LEAL, L. G. 1980 Particle motion in a viscous fluid. *Annu. Rev. Fluid Mech.* **12**, 435–476.

LUO, L.-S. 1998 Unified theory of the lattice Boltzmann models for nonideal gases. *Phys. Rev. Lett.* **81**, 1618–1621.

Luo, L.-S. 2000 Theory of lattice Boltzmann method: Lattice Boltzmann models for nonideal gases. *Phys. Rev.* E **62**, 4982–4996.

McNamara, G. & Zanetti, G. 1988 Use of Boltzmann equation to simulate lattice-gas automata. *Phys. Rev. Lett.* **61**, 2332–2335.

Poe, G. G. & Acrivos, A. 1975 Closed-streamline flows past rotating single cylinders and spheres: inertial effect. *J. Fluid Mech.* **72**, 605.

Qi, D. W. 1997a Non-spheric colloidal suspensions in three-dimensional space. *Intl J. Mod. Phys.* C **8**, 985–997.

Qi, D. W. 1997b Computer simulation of coating suspensions. *Proc. Tappi Advanced Coating Fundamental Symp. May, Philadelphia, PA*, pp. 201–211.

Qi, D. W. 1999 Lattice Boltzmann simulations of particles in non-zero-Reynolds-number flows. *J. Fluid Mech.* **385**, 41–62.

Qi, D. W. 2000 Lattice Boltzmann simulations of fluidization of rectangular particles. *Intl J. Multiphase Flow* **26**, 421–433.

Qi, D. W. 2001 Simulations of fluidization of cylindrical particles in a three-dimensional space. *Intl J. Multiphase Flow* **27**, 107–118.

Qi, D. W. & Luo, L. S. 2002 Transitions in rotations of a non-spherical particle in a three-dimensional moderate-Reynolds-number Couette flow. *Phys. Fluids* **14**, 4440–4443.

Qian, Y., d'Humières, D. & Lallemand, P. 1992 Lattice BGK models for Navier–Stokes equation. *Europhys. Lett.* **17**, 479–484.

Saffman, P. G. 1965 The lift on a small sphere in a slow shear flow. *J. Fluid Mech.* **22**, 385–400.

Taylor, G. I. 1923 The motion of ellipsoidal particles in a viscous fluid. *Proc. R. Soc. Lond.* A **102**, 58–61.

Zettner, C. M. & Yoda, M. 2000 The circular cylinder in simple shear at moderate Reynolds numbers: An experimental study. *Exps. Fluids* **30**, 346–353.

Zettner, C. M. & Yoda, M. 2001 Moderate-aspect-ratio elliptical cylinders in simple shear with inertia. *J. Fluid Mech.* **442**, 241–266.